Joule

CellPress
OPEN ACCESS

Article

Three-dimensional multi-layer carbon tube electrodes for AC line-filtering capacitors

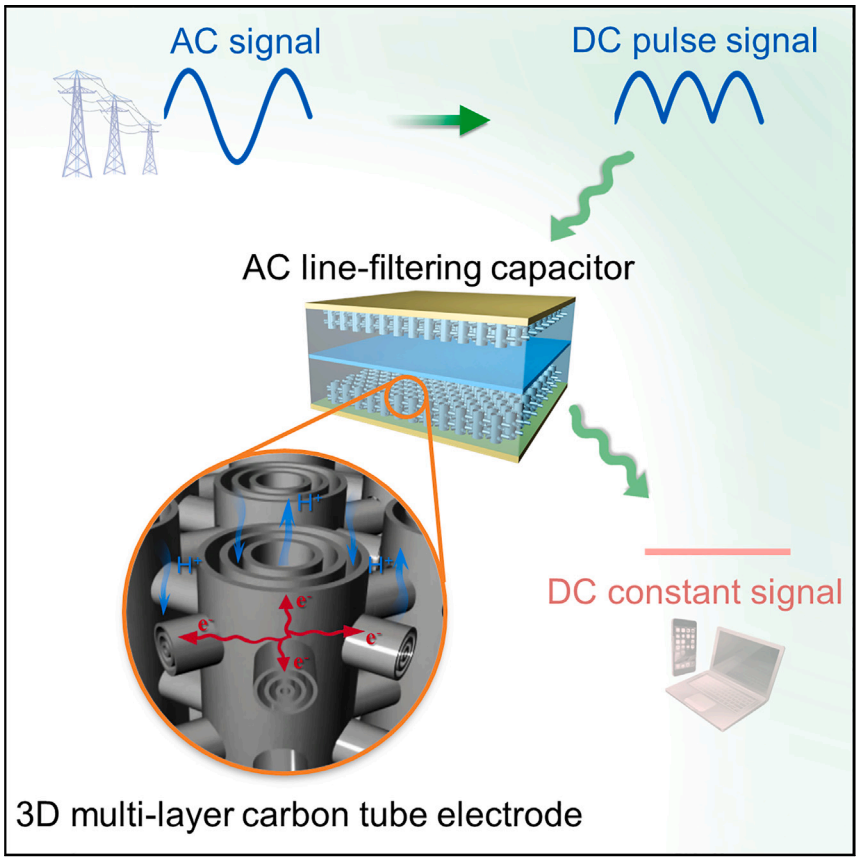

High areal specific capacitance and fast frequency response electric double-layer capacitors are achieved based on a three-dimensional multi-layer carbon tube (3D-MLCT) framework, showing excellent AC line-filtering performance. The unique hollow tube-in-tube structure of the 3D-MLCT provides abundant ion adsorption surface and fast ion migration channels, which is promising for miniaturized circuit filter devices.

Gan Chen, Fangming Han, Dou Lin, ..., Xiaoguang Zhu, Guowen Meng, Bingqing Wei

fmhan@issp.ac.cn (F.H.)
gwmeng@issp.ac.cn (G.M.)
weib@udel.edu (B.W.)

Highlights

3D multi-layer carbon tube electrodes are fabricated for AC line-filtering capacitors

Single-layer, double-layer, and triple-layer carbon tube frameworks are realized

The inter-layer spacings of multi-layer carbon tubes can be precisely controlled

The unique structure contributes to high capacitance and fast frequency response

Chen et al., Joule *8*, 1–12
April 17, 2024
https://doi.org/10.1016/j.joule.2024.01.026

Please cite this article in press as: Chen et al., Three-dimensional multi-layer carbon tube electrodes for AC line-filtering capacitors, Joule (2024), https://doi.org/10.1016/j.joule.2024.01.026

Joule

CellPress
OPEN ACCESS

Article

Three-dimensional multi-layer carbon tube electrodes for AC line-filtering capacitors

Gan Chen,[1,2] Fangming Han,[1,2,*] Dou Lin,[1,2] Shiping Zhang,[1,2] Qijun Pan,[1,2] Cheng Shao,[1] Zhaoming Wang,[1] Xiaoguang Zhu,[1] Guowen Meng,[1,2,4,*] and Bingqing Wei[3,*]

SUMMARY

Electric double-layer capacitors (EDLCs) have the potential to replace aluminum electrolytic capacitors for alternating current line-filtering, aligning with the trend of device miniaturization. However, it is challenging for EDLCs to simultaneously achieve rapid ion migration, electrical response, and high areal and volumetric capacitances. Here, we demonstrate that three-dimensional, structurally integrated multi-layer carbon tube (3D-MLCT) frameworks are used as electrodes for high-performance filtering EDLCs. By simply increasing the number of tube layers, a high specific areal capacitance of 3.08 mF cm^{-2} at 120 Hz is achieved with a phase angle of −80.1°, exhibiting excellent capacitance and fast frequency response. The outstanding performance of the 3D-MLCT is attributed to the high density, high orientation, and high integrality of carbon tube arrays that facilitate and accelerate ion distribution onto the electrode surface. The findings of this work provide a solution for developing next-generation miniaturized filter capacitors with high capacitance and fast frequency response.

INTRODUCTION

Converting alternating current (AC) into direct current (DC) is essential for powering electronics.[1–3] In the process, filter capacitors play a crucial role in smoothing the ripples in the rectified DC signal.[4–7] Aluminum electrolytic capacitors (AECs) dominate this field but occupy the most significant volume in circuits.[8–10] Electric double-layer capacitors (EDLCs), storing energy physically through reversible ion adsorption at the electrode-electrolyte interface, have been anticipated for fast frequency response applications.[11–15] EDLCs are considered promising alternative devices for AC line-filtering to meet the demands of miniaturized electronic devices owing to their several-orders-of-magnitude-higher specific capacitance than commercial AECs.[16–23] However, conventional EDLCs behave more like resistors than capacitors and possess poor frequency response performance at an indicator frequency of 120 Hz because of their tortuous and complicated pore structure as well as the high resistances of the electrodes.[24–27]

The first filtering EDLC was reported by Miller et al.,[1] with discrete vertically oriented graphene (VOG) nanosheets grown on nickel substrates as electrodes, demonstrating an outstanding AC line-filtering performance. Subsequently, various carbon-nanomaterial-based electrodes with high orientation, thin thickness, and macro-porous structures have been explored for filtering EDLCs.[28–35] However,

CONTEXT & SCALE

Alternating current line-filtering capacitors are critical for digital circuits and electronics. Aluminum electrolytic capacitors (AECs) are the most used filter capacitors, but their bulky size has hindered their application in miniaturization. Electric double-layer capacitors (EDLCs), whose capacitance is much higher than AECs, are expected to be miniaturized filter capacitors. However, achieving EDLCs with high-frequency and high-capacitance performances is challenging. Designing high-oriented and high-density carbon-based electrodes would minimize the performance trade-off between frequency response and capacitance.

We report three-dimensional multi-layer carbon tube electrodes for miniaturized filter capacitors, and the structure of the electrodes can be precisely controlled. These capacitors exhibit desirable capacitance for carbon nanotube-based EDLCs and excellent filtering characteristics for line-filtering applications and could be integrated into miniaturized devices.

Please cite this article in press as: Chen et al., Three-dimensional multi-layer carbon tube electrodes for AC line-filtering capacitors, Joule (2024), https://doi.org/10.1016/j.joule.2024.01.026

the specific areal (C_A) and volumetric capacitances (C_V) are still at a low level—the bottleneck of miniaturized filter devices.[36–39]

Recently, we have demonstrated three-dimensional carbon tube (3D-CT) grid-based electrodes with integrated structures for line-filtering applications.[2] The 3D-CT grids, employed as the electrodes of EDLCs, showed exceptional line-filtering capabilities owing to their 3D-ordered design, functional CT units, chemical bond connections, high conductivity, stable open-pore structures, and interconnected lateral and vertical carbon tubes that facilitate smooth ion distribution channels. The preliminary results reported of filling CTs with smaller-diameter carbon nanotubes (CNTs) (3D-CNT@CT) have blazed a trail in enhancing C_A effectively. However, due to the relatively sparse distribution and unoriented alignment of smaller CNTs inside the CTs, the increase in C_A is limited, and the rapid migration of ions inside CTs is hindered. To further improve C_A to meet the expectations of miniaturized filter capacitors, the CTs could be uniformly filled with concentric tubes that replicate their original morphology to provide rich ion-accessible surface areas while maintaining the high orientation of the interconnected structure. This kind of "tube nested inside tube" functional unit, similar to Russian matryoshka dolls, could be combined in an orderly manner to obtain a unique 3D-CT-based framework with a controllable number of CT layers and inter-layer spacing. Therefore, filling multi-layered CTs (vertical and lateral) within the initially integrated 3D-CTs would be an attractive and rational design to significantly increase the C_A without degrading the frequency response performance.

Herein, we report structurally integrated 3D multi-layer CT (denoted as 3D-MLCT) frameworks that are used as electrodes for high-performance line-filtering EDLCs, showing high C_A and fast frequency response capability. The 3D-MLCT framework was fabricated via a combinational process with a 3D porous anodic aluminum oxide (3D-AAO) as a template, including chemical vapor deposition (CVD) of CTs in the 3D pores of 3D-AAO, atomic layer deposition (ALD) of an alumina layer as the sacrificial material, CVD of inner CTs, and then chemically etching the alumina layer and the 3D-AAO template. 3D single-layer, double-layer, and triple-layer CT frameworks (denoted as 3D-SLCT, 3D-DLCT, and 3D-TLCT) have been constructed by controlling the number of layers. The 3D-TLCT-based EDLC exhibits a desirable C_A value of about 3.08 mF cm^{-2} at 120 Hz with a phase angle below −80°, over 70% higher than the value of 3D-CNT@CT (1.81 mF cm^{-2}).[2] To verify practicability, ten EDLCs based on the 3D-MLCTs assembled in series to filter a rectified 120-Hz pulse DC signal and a pulse voltage signal generated from a triboelectric nanogenerator (TENG) have shown gratifying line-filtering performances. The excellent performances of the 3D-MLCT-based EDLCs are attributed to the high density, orientation, and integrality of the 3D-ordered structure composed of functional MLCT units that facilitate and accelerate ion distribution onto the electrode surface. The findings of this work provide a unique solution for developing next-generation miniaturized line-filter capacitors with high capacitance and fast frequency response.

RESULTS AND DISCUSSION

The fabricating process of 3D-MLCT is schematically illustrated in Figure 1. A 3D-AAO template with interconnected vertical and lateral channels was synthesized by anodizing impure aluminum foil in phosphoric acid electrolyte at 0°C under a voltage of 195 V (Figure S1).[40,41] The template was placed into a horizontal tube furnace and heated to 1,000°C at 10°C/min under an Ar atmosphere. The first CT

[1]Key Laboratory of Materials Physics and Anhui Key Laboratory of Nanomaterials and Nanotechnology, Institute of Solid State Physics, HFIPS, Chinese Academy of Sciences, Hefei 230031, China

[2]Department of Materials Science and Engineering, University of Science and Technology of China, Hefei 230026, China

[3]Department of Mechanical Engineering, University of Delaware, Newark, DE 19716, USA

[4]Lead contact

*Correspondence: fmhan@issp.ac.cn (F.H.), gwmeng@issp.ac.cn (G.M.), weib@udel.edu (B.W.)

https://doi.org/10.1016/j.joule.2024.01.026

Please cite this article in press as: Chen et al., Three-dimensional multi-layer carbon tube electrodes for AC line-filtering capacitors, Joule (2024), https://doi.org/10.1016/j.joule.2024.01.026

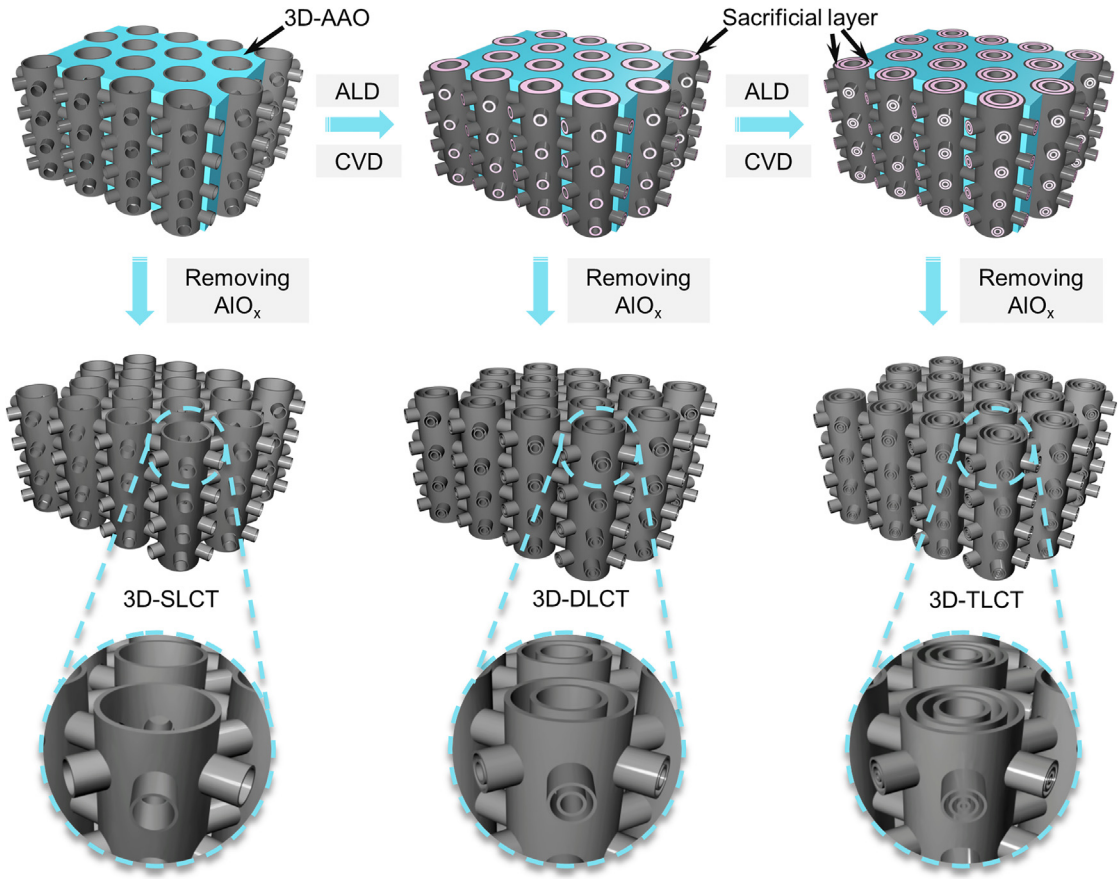

Figure 1. Schematic illustration of the synthesis process of the 3D-SLCT, 3D-DLCT, and 3D-TLCT

layer was deposited on the pore walls of the 3D-AAO template with a flow of acetylene gas under vacuum conditions for 50 min. Subsequently, an AlO_x layer was deposited via an ALD process at 250°C on the inner wall of the first CT layer using trimethyl aluminum (TMA) and ozone (O_3) as the precursors.[42] The second CT layer was deposited on the AlO_x surface via a second-time CVD process. Similarly, repeating the ALD and subsequent CVD processes can prepare a third CT layer. Finally, the 3D-MLCT was obtained after removing the AlO_x layer(s) and 3D-AAO template in hydrofluoric acid solution, and the spacing of adjacent CT layers can be precisely controlled by the thickness of the AlO_x layers. Furthermore, the size of the 3D-CT films can be adjusted by varying the area of the 3D-AAO as needed, and we prepared a 3D-CT film with an area of approximately 24 cm^2 (see Figure S2).

The representative scanning electron microscopy (SEM) image (Figure 2A) reveals that the 3D-MLCT with a unique coaxial tube-in-tube structure was successfully prepared without agglomeration of the CTs, and the uniformity of the structure is notably high. The lateral CT connections make the 3D-MLCT framework form an integrated and freestanding film with a uniform thickness (Figures 2B–2F), which is the same as the 3D-AAO template and can be adjusted by the anodizing time (Figure S3). The lateral and the vertical tubes are well connected, and the inner CT layers possess the same 3D interconnected structure as the outer layer (Figures 2D–2F). The detailed designs are confirmed by the transmission electron microscopy (TEM) images (Figures 2G–2I).

Please cite this article in press as: Chen et al., Three-dimensional multi-layer carbon tube electrodes for AC line-filtering capacitors, Joule (2024), https://doi.org/10.1016/j.joule.2024.01.026

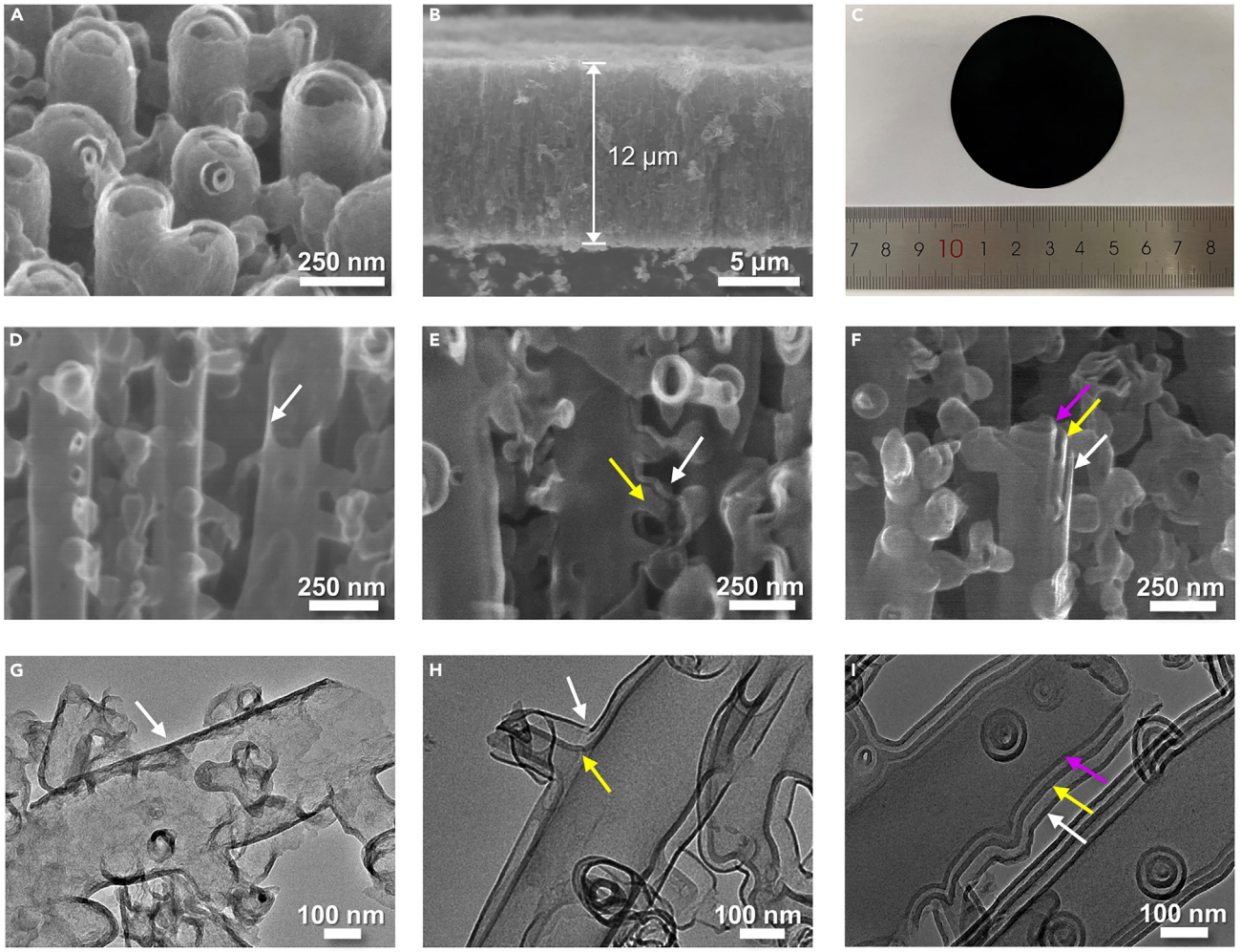

Figure 2. Morphological and structural characteristics of the 3D-SLCT, 3D-DLCT, and 3D-TLCT

(A) Top-view SEM image of 3D-DLCT.

(B) Typical cross-section SEM image of 3D-DLCT.

(C) Optical image of a freestanding 3D-CT film.

(D–F) Enlarged cross-section SEM images of (D) 3D-SLCT, (E) 3D-DLCT, and (F) 3D-TLCT.

(G–I) TEM images of (G) 3D-SLCT, (H) 3D-DLCT, and (I) 3D-TLCT.

The inter-layer spacings of the 3D-MLCT frameworks could be finely regulated by controlling the thicknesses of the AlO_x sacrificial layers, and the inter-layer spacing of approximately 12 and 36 nm corresponds to 100 and 300 ALD cycles, respectively (Figures 3A and 3B). The N_2 adsorption-desorption analysis was utilized to evaluate the specific surface area (SSA) and pore structure of as-prepared 3D-SLCT, -DLCT, and -TLCT films (Figures 3C and S4, and supplemental information). All the samples exhibit typical type IV isotherms with no obvious inflection point at low pressure and an H3-type hysteresis loop at higher relative pressure, illustrating the hierarchical porous structure and the existence of abundant meso/macropores. The 3D-SLCT, -DLCT, and -TLCT films show a Braunauer-Emmett-Teller (BET) volumetric SSA of 16.4, 33.8, and 45.0 m^2/cm^3, respectively. The volumetric SSA increases almost linearly with the number of layers, confirming the unique multi-layer structure's crucial role in effectively improving the distribution density of CTs per unit volume and enhancing the mass loading. In addition, the electrochemical surface area measurements of the 3D-MLCT films were conducted to estimate the SSA per footprint area

Please cite this article in press as: Chen et al., Three-dimensional multi-layer carbon tube electrodes for AC line-filtering capacitors, Joule (2024), https://doi.org/10.1016/j.joule.2024.01.026

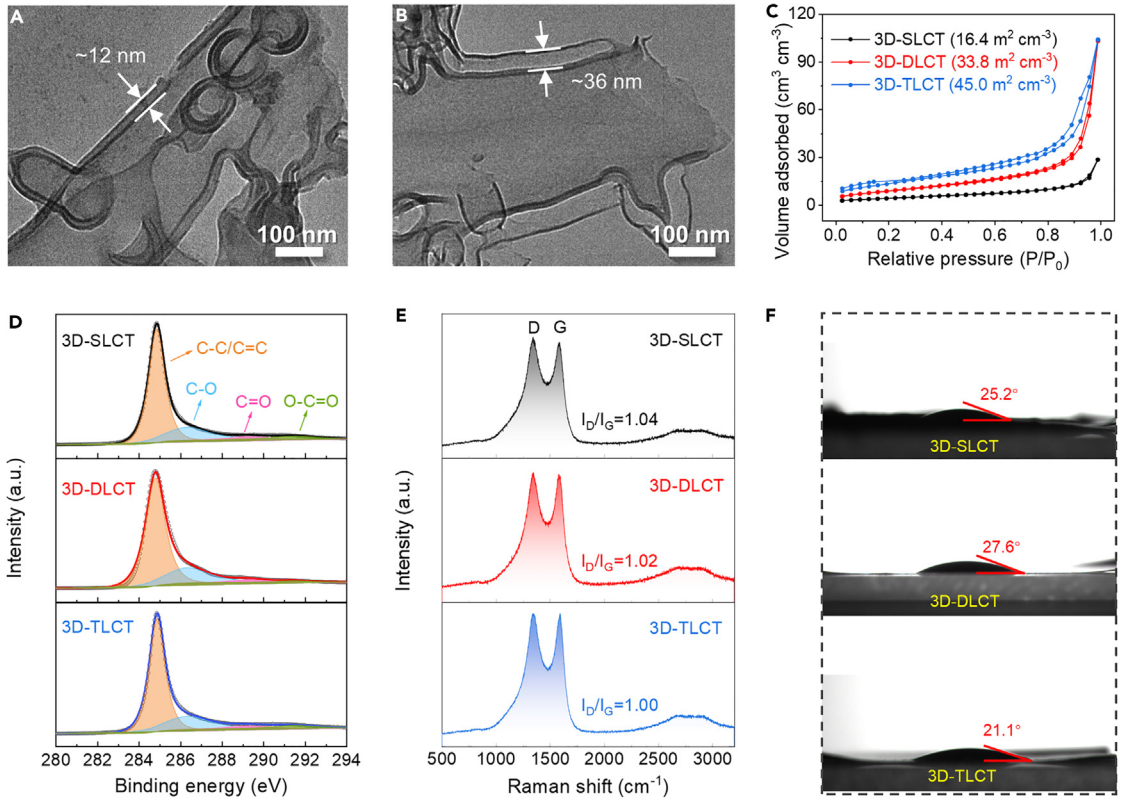

Figure 3. Structural and compositional characterizations of the 3D-SLCT, 3D-DLCT, and 3D-TLCT

(A and B) TEM images of 3D-DLCT with different inter-layer spacings of (A) 12 and (B) 36 nm, respectively.

(C) Nitrogen adsorption-desorption isotherms of the 3D-SLCT, 3D-DLCT, and 3D-TLCT.

(D) C 1s XPS spectra of the 3D-SLCT, 3D-DLCT, and 3D-TLCT films.

(E) Raman spectrum of the 3D-SLCT, 3D-DLCT, and 3D-TLCT films.

(F) Contact angle tests of the 3D-SLCT, 3D-DLCT, and 3D-TLCT films.

(cm^2 per cm^2) by measuring the double-layer capacitance and factoring in the roughness (Figure S5). The roughness factors for 3D-SLCT, DLCT, and TLCT were determined to be 204.2, 333.3, and 508.3 cm^2 cm^{-2}, respectively, consistent with the trend observed in the BET testing results. The surface elemental configurations of 3D-MLCT films were investigated by X-ray photoelectron spectroscopy (XPS) characterizations. Characteristic peaks at binding energies of 284.8, 286.3, 289.3, and 291.5 eV are shown in the high-resolution C1s spectrum (Figure 3D), which corresponded to C–C/C=C, C–O, C=O, and O–C=O bonds, respectively.[43] The relatively low O/C element ratios indicate fewer oxygen-containing functional groups on the surface of the prepared electrode films. Raman spectra were carried out to verify the degree of defect of the above carbon films. Figure 3E shows the typical characteristic D band (~1,350 cm^{-1}) and G band (~1,580 cm^{-1}) in Raman spectroscopy.[44,45] The comparable intensity ratios of the D/G band (I_D/I_G) indicate that the number of layers did not significantly affect the graphitization degree. Moreover, the surface defects will improve the wettability of these carbon electrodes in aqueous electrolytes, as shown in small contact angles (Figure 3F), which will be beneficial to facilitating ion accessibility and reducing the interfacial impedance.[11]

Symmetrical cells with a two-electrode configuration were constructed using the 3D-CT films as electrodes, platinum sheets as the current collectors, and a 1M H_2SO_4 aqueous solution as the electrolyte (Figure S6). The electrochemical energy storage,

Please cite this article in press as: Chen et al., Three-dimensional multi-layer carbon tube electrodes for AC line-filtering capacitors, Joule (2024), https://doi.org/10.1016/j.joule.2024.01.026

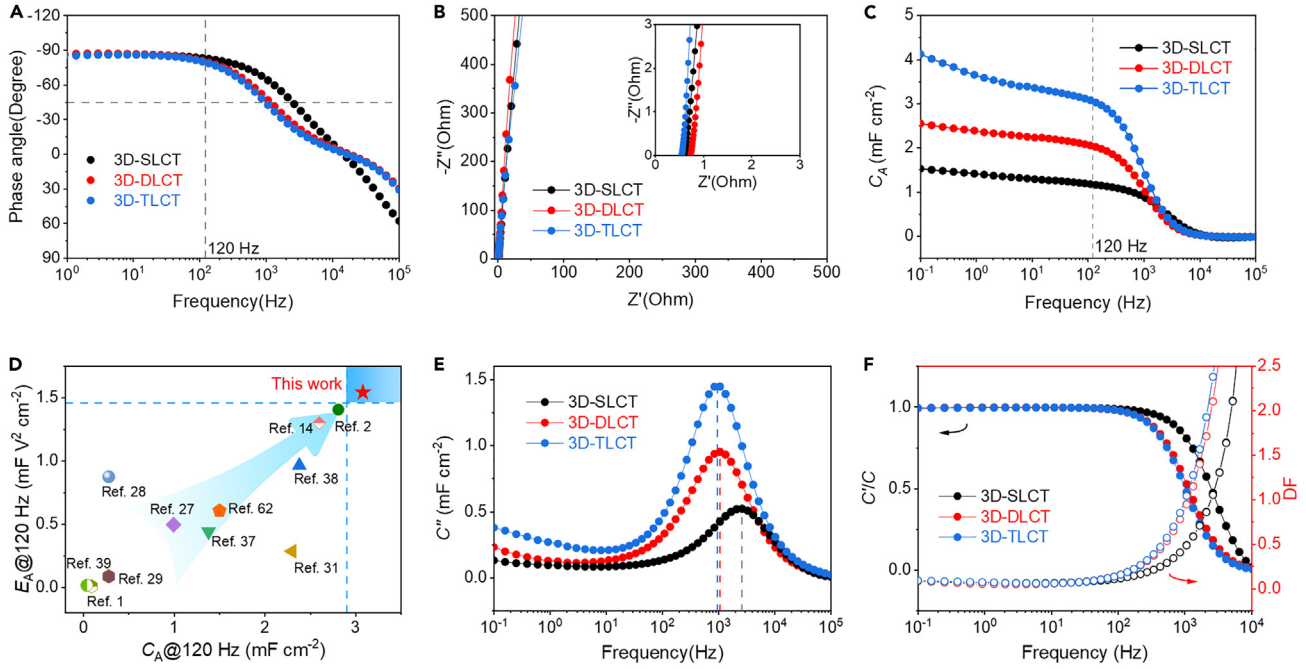

Figure 4. The electrochemical performances of the 3D-SLCT-, 3D-DLCT-, and 3D-TLCT-based EDLCs

(A–C) (A) Bode plots, (B) Nyquist plots, and (C) specific areal capacitance (C_A) of the 3D-SLCT-, 3D-DLCT-, and 3D-TLCT-based EDLCs. The inset shows the expanded view at high frequencies.

(D) Comparison of C_A and areal specific energy density (E_A) of the 3D-TLCT-based EDLC at 120 Hz, with other reported aqueous electrochemical capacitors with a symmetric sandwich-type device configuration used in the AC filter circuits.

(E) Plots of the imaginary part of the specific capacitance (C'') versus frequency based on the series-RC circuit model.

(F) The variation of C'/C and dissipation factor versus frequency.

cycling performance, and Coulombic efficiency of the 3D-DLCT-based EDLCs were investigated (Figures S7–S9), demonstrating an ideal capacitive behavior and remarkable cycle/rate stability. The performances of 3D-DLCT with different inter-layer spacings (denoted as 3D-DLCT-12, -24, and -36, the last numbers represent the inter-layer spacing [in nanometers]) have been studied, proving that C_A increases with the decrease of the inter-layer spacing (Figure S10). Properties of 3D-DLCT-24 with different thicknesses of 7.5, 12, and 14 μm were tested to investigate the effect of electrode thickness on the electrochemical and AC line-filtering performance (Figure S11). The 3D-DLCT-24-based EDLC with an electrode thickness of 12 μm can achieve both a low phase angle (<−80°) and a high C_A (>2 mF cm^{-2}), demonstrating an outstanding application potential for AC line-filtering, so this thickness is selected in the subsequent tests.

For comparison, the 12-μm-thick 3D-SLCT, 3D-DLCT, and 3D-TLCT films were assembled into symmetrical EDLC devices, respectively. The phase angles of these EDLCs at low frequencies are close to −90°, reflecting the characteristics of ideal capacitors (Figure 4A). f_{-45}, the frequency at which the phase angle is −45°, is the cut-off value to distinguish a capacitor's capacitive and resistive behaviors.[46] f_{-45} is commonly used to evaluate the frequency performance of line-filtering capacitors.[1] A capacitor with a higher f_{-45} indicates a faster response at high frequencies for line-filtering capacitors.[17] The f_{-45} of the 3D-SLCT-, 3D-DLCT-, and 3D-TLCT-based EDLCs are 2,595, 1,068, and 951 Hz, respectively, much higher than that of traditional EDLCs.[26,47] The phase angle at 120 Hz is deemed a factor of merit for the AC line-filtering capacitors.[48] As shown in the Bode plot in Figure 4A, the phase

Please cite this article in press as: Chen et al., Three-dimensional multi-layer carbon tube electrodes for AC line-filtering capacitors, Joule (2024), https://doi.org/10.1016/j.joule.2024.01.026

angles at 120 Hz of the above devices are −83.3°, −81.0°, and −80.1°, respectively. The results reveal that these EDLCs exhibit excellent frequency response performances, comparable to those of AEC (−83.5°, Panasonic Japan, 330 μF, 6.3V, Figure S12), indicating that the EDLCs have low electron and ion resistances in the 3D-CT frameworks. Moreover, the ion transport channels are more complex when the layer number increases, showing higher phase angles. The Nyquist plots of the above EDLCs are shown in Figure 4B. The curves are nearly perpendicular to the real axis, revealing their pure double-layer capacitive behaviors,[49] and no apparent porous effect was observed.[50] All the 3D-CT-based EDLCs show a small equivalent series resistance (ESR), which can be attributed to the excellent electrical conductivity of the 3D-MLCT and the good contact with the current collectors. These results indicate that the double-layer and triple-layer CT frameworks allow fast ion distribution and electron conduction dynamics, provided by the ordered smooth pore channels and high conductivity of the 3D-CT frameworks.

The frequency-dependent capacitive behavior is further analyzed using the complex capacitance concept. The real part of the capacitance (C') represents the actual accessible energy at the corresponding frequency, while the imaginary part (C'') is caused by energy dissipation due to resistive diffusion and leakage currents (calculations in supplemental information).[51,52] At 120 Hz, the C_A (i.e., the areal C') of the 3D-SLCT-, 3D-DLCT-, and 3D-TLCT-based EDLCs can achieve 1.18, 2.05, and 3.08 mF cm^{-2}, respectively (Figure 4C). The influence of parasitic capacitance is excluded by measuring capacitance without the 3D-MLCT electrodes (Figure S13). The areal specific energy density (E_A) at 120 Hz of 3D-TLCT-based EDLC is calculated to be about 1.54 mF V^2 cm^{-2}, greater than most aqueous filtering capacitors with sandwich-type configurations reported to date (Figure 4D; Table S1). The high C_A and E_A indicate that the 3D-TLCT-based EDLC has a capacitance advantage compared with other reported filter capacitors (with a phase angle < −80° at 120 Hz), proving that the hollow multi-layer structure plays a key role in enhancing the capacitance without affecting the frequency response.[53,54] The C_A of the 3D-MLCT-based EDLCs is substantially 2 orders of magnitude higher than those of commercial AECs (around 0.08 mF cm^{-2}) and increases with the increase of the layer number. Additionally, the C_A exhibits little loss with increasing frequency in the low-frequency region, revealing the fast frequency response and excellent capacitance retention capability. The C_V at 120 Hz can achieve 1.28 F cm^{-3} for the 3D-TLCT electrodes (Figure S14). The resistor-capacitor (RC) time constant (τ_{RC}) is a characteristic parameter of EDLCs and reflects how fast the capacitor can be charged/discharged.[50,55,56] The τ_{RC} of the 3D-SLCT-, 3D-DLCT-, and 3D-TLCT-based EDLCs at 120 Hz is 0.17, 0.24, and 0.25 ms, respectively, comparable to that of AEC (0.17 ms). The characteristic frequency (f_0) can be gained at the maximum point of C'',[52] corresponding to the relaxation time constant τ_0, the minimum time required for the capacitors to discharge with an energy efficiency of over 50%,[45] which is 0.38, 0.94, and 1.05 ms, respectively for the 3D-SLCT-, 3D-DLCT-, and 3D-TLCT-based EDLCs (Figure 4E). The relatively low τ_0 values mean that the 3D-MLCT electrodes hold the fast frequency response ability.[1] The frequency-dependent C'/C value, representing the ratio of the actual storage capacity to the total capacity, is close to 1 at 120 Hz (Figure 4F), indicating that the capacitors would not cause excessive energy loss during the working process and that the actual energy storage efficiency is high. This is consistent with the dissipation factor (DF) result, whose value is minimal at a low-frequency region (Figure 4F), suggesting the slight loss characteristic and ideal capacitive behavior of the 3D-MLCT-based EDLCs.[57,58]

Please cite this article in press as: Chen et al., Three-dimensional multi-layer carbon tube electrodes for AC line-filtering capacitors, Joule (2024), https://doi.org/10.1016/j.joule.2024.01.026

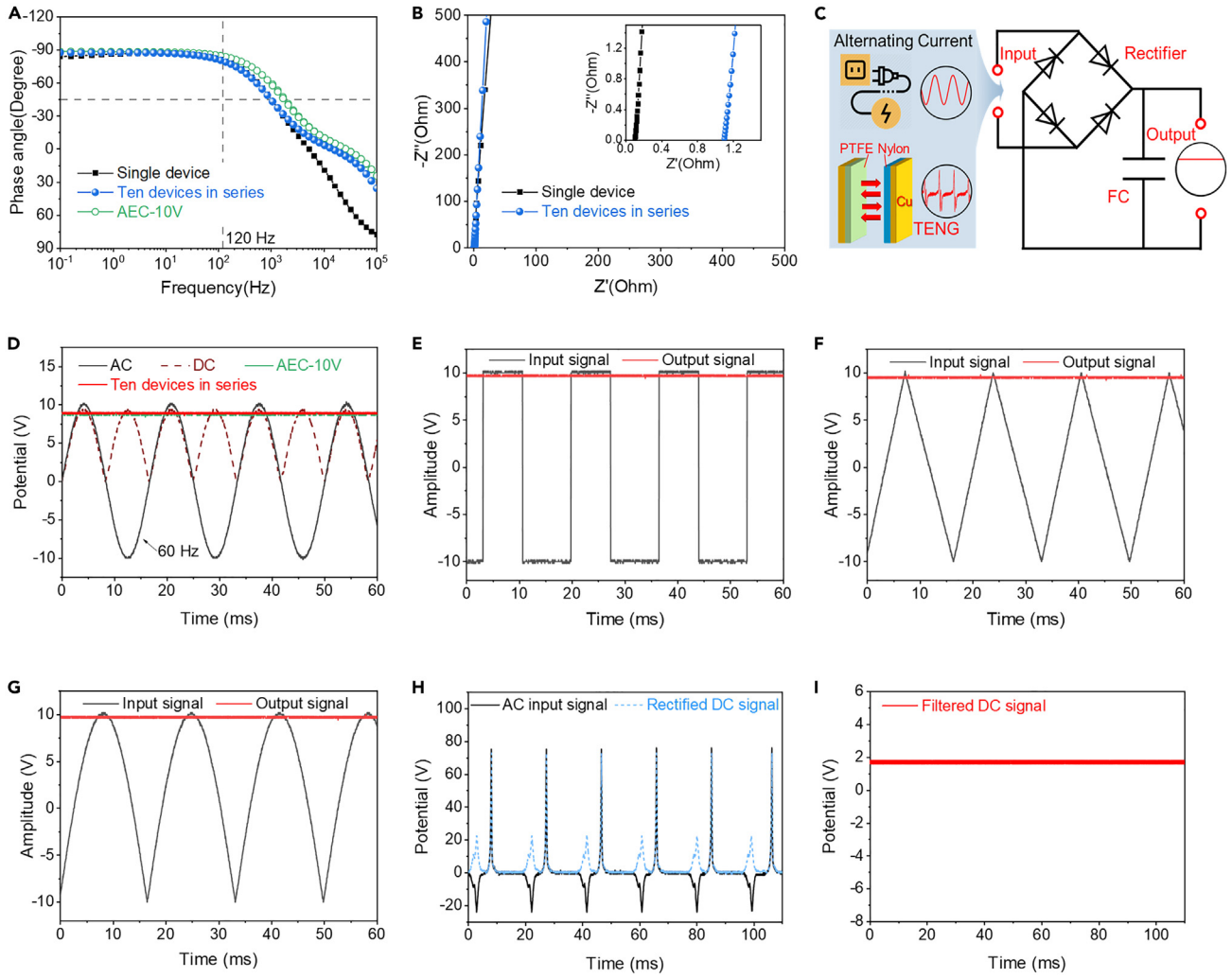

Figure 5. The electrochemical performances of single EDLC, ten EDLCs in series, and the AC line-filtering performance demonstration

(A) Bode plots.

(B) Nyquist plots.

(C) Schematic of the rectifier and filter circuit powered by AC voltage and TENG pulse voltage.

(D) AC line-filtering results of ten EDLCs in series and commercial AEC (10 V/100 μF, Nippon, Japan) with R_L of 100 kΩ.

(E–G) The filtering performances of the 3D-DLCT-24-based EDLCs for 60 Hz AC input signals with (E) square, (F) triangular, and (G) arbitrary waveforms.

(H and I) Electrical signals powered by TENG at (H) initial AC state, rectified state, and (I) filtered DC state.

To create a more realistic comparison, ten identical 3D-DLCT-24-based capacitors (with an electrode area of ~1 cm^2 and thickness of 10 μm) were connected in series to expand the operating voltage to 10 V compared with the standard 10-V AECs. The individual devices can be arranged separately or stacked in series (Figure S15). The EDLCs in the series show a close-to-ideal capacitive behavior (Figures S16A and S16B). The four-electrode test was adopted to evaluate the EIS of the EDLCs in series. The phase angles at 120 Hz of ten devices in series achieve −80.7°, comparable to that of the single device (−81.5°) and slightly inferior to the AEC (−84.8°) (Figure 5A). The ESR increases nearly proportionally with the number of units in series (Figure 5B), which were accompanied by a related augmentation in capacitive reactance (*Xc*) (Table S2), thus affecting the frequency response performance negligibly.[2] The τ_{RC} of the capacitor bank (0.24 ms) is comparable to that of the single device (0.23 ms) and the AEC (0.13 ms). The capacitance of a single device is about ten

Please cite this article in press as: Chen et al., Three-dimensional multi-layer carbon tube electrodes for AC line-filtering capacitors, Joule (2024), https://doi.org/10.1016/j.joule.2024.01.026

times that of the devices in series, which conforms to the law of capacitors in series (Figure S16C). The capacitance of the 10 devices in series (143 μF) is higher than that of commercial AEC (100 μF). Also, the same τ_0 value of 0.96 ms is observed, confirming that good frequency response performance can be maintained by connecting EDLCs in series. The C'/C values are close to 1 at 120 Hz, indicating low energy loss and high practical energy storage efficiency, consistent with the results of the relatively low *DF* value (Figure S16D). It should be noted that the *DF* of the capacitor bank is still relatively high compared with commercial AECs, but this can be improved by reducing the thickness of the 3D-DLCT electrodes (Figure S17). These measurements suggest that the high-frequency response and rate capability performance of 3D-DLCT-24-based EDLCs are maintained well when working in the serial connection.

The volumetric capacitance at rated voltage ($C_{V\ vol}$) of 3D-DLCT-based EDLCs was compared with commercial AECs.[59] The calculated $C_{V\ vol}$ for the 3D-DLCT-based EDLCs in the aqueous electrolyte is $0.15/V^2$, where V is the voltage rating (based on the device's volume, supplemental information).[28,60] 3D-DLCT-based EDLCs can be connected in series to achieve a higher operating voltage. The volumetric capacitance is higher at operating voltages of <16 V than commercial AECs. The operating voltage of a single EDLC can be increased when an organic electrolyte is used, and the EDLC also shows a high capacitive and filtering performance (Figures S18 and S19). $C_{V\ vol}$ will increase to $0.70/V^2$, and the 3D-DLCT-based EDLCs have volumetric advantages over commercial AECs at voltages of <100 V (Figure S20).

A filter circuit employing ten 3D-DLCT-24-based EDLCs in series (Figure 5C) was built to verify their AC line-filtering performances. The input 60-Hz AC signal is converted into a 120-Hz sinusoidal signal without negative voltage by the full-bridge rectifier. The rectified signal is further smoothed into a constant DC signal required by the electrical appliances. Figure 5D shows that the AC input signals (±10 V of the peak voltage) with a loading resistance (R_L) of 100 kΩ can be filtered into the DC output with a trivial ripple voltage, which is comparable to that of AEC (10 V/100 μF, Nippon, Japan), and demonstrates the potential applicability of the 3D-DLCT-24-based EDLCs used as filter capacitors at relatively high voltages. Under different high loadings, the capacitor banks in series exhibit comparable output voltages and small variance coefficients compared with AECs (Figure S21). However, when R_L is too small (such as 100 and 470 Ω), a significant 120-Hz ripple voltage is displayed (Figure S22). Different types of input signals, including square, triangular, and arbitrary waveforms (Figures 5E–5G), can also be filtered into smooth DC output signals without visible ripples. The high specific capacitance, low ESR, and small τ_{RC} of the 3D-DLCT-based EDLCs guarantee promising prospects in fabricating practical high-frequency devices with prosperous filtering functions.

A TENG[61] was designed to generate pulsed voltage signals and simulate the environmental pulsed energy to demonstrate the practical application potential of 3D-DLCT-based EDLCs as a filtering capacitor (Figure 5C). The performance for capturing intermittent energy, smoothing the pulsed voltage, and driving a light-emitting diode (LED) of the 3D-DLCT-24-based EDLCs is investigated.[50,62] The bi-directional pulse voltage generated by the TENG is passed through a bridge rectifier and filtered by the 3D-DLCT-24-based EDLCs in series. The rectified ripple voltage signal is smoothed (Figures 5H and 5I), and the LED is lit stably and continuously under a consistent power supply rather than frequently flickering without the EDLCs (relevant displays can be seen in Figure S23; Video S1). In addition, the meager

charge of the TENG could be quickly absorbed by the capacitors, thus preventing them from being broken down by the instantaneous high voltage (>70 V).[50]

In summary, structurally integrated, freestanding 3D-MLCT frameworks with multi-layered tube-in-tube structures were fabricated by a combinatorial process of alternating CVD and ALD using a 3D-AAO template and subsequent selective etching. EDLCs based on the 3D-TLCTs exhibit a large areal specific capacitance of 3.08 mF cm^{-2} and a phase angle of −80.1° at 120 Hz, demonstrating excellent frequency response performances. High voltage filter capacitors can be achieved by connecting the EDLCs in series. The results provide a solution for developing next-generation miniaturized filter capacitors with high capacitance and fast frequency response.

EXPERIMENTAL PROCEDURES

Resource availability

Lead contact

Further information and requests for resources and materials should be directed to and will be fulfilled by the lead contact, Guowen Meng (gwmeng@issp.ac.cn).

Materials availability

The materials in this study will be made available upon reasonable request.

Data and code availability

The published article includes all data generated or analyzed during this study.

For full details, please refer to supplemental experimental procedures.

SUPPLEMENTAL INFORMATION

Supplemental information can be found online at https://doi.org/10.1016/j.joule.2024.01.026.

ACKNOWLEDGMENTS

This work was supported by the National Natural Science Foundation of China (91963202, 52072372, 52372241, and 52232007), HFIPS Director's Fund (BJPY2023A07 and YZJJ-GGZX-2022-01), and Key Research Program of Frontier Sciences (CAS, grant QYZDJ-SSW-SLH046).

AUTHOR CONTRIBUTIONS

G.M., B.W., and F.H. designed and supervised the project. G.C. developed the idea and performed the experiment. D.L., S.Z., Q.P., C.S., Z.W., and X.Z. helped with the material characterization. G.C., F.H., G.M., and B.W. wrote the manuscript. All authors discussed the results and approved the final version of the manuscript.

DECLARATION OF INTERESTS

A Chinese patent has been submitted in relation to this work (ZL 2022 1 0856006.3).

Received: September 24, 2023
Revised: December 28, 2023
Accepted: January 25, 2024
Published: February 15, 2024

REFERENCES

1. Miller, J.R., Outlaw, R.A., and Holloway, B.C. (2010). Graphene double-layer capacitor with ac line-filtering performance. Science *329*, 1637–1639.
2. Han, F., Qian, O., Meng, G., Lin, D., Chen, G., Zhang, S., Pan, Q., Zhang, X., Zhu, X., and Wei, B. (2022). Structurally integrated 3D carbon tube grid-based high-performance filter capacitor. Science *377*, 1004–1007.
3. Park, J., and Kim, W. (2021). History and Perspectives on Ultrafast Supercapacitors for AC Line Filtering. Adv. Energy Mater. *11*, 2003306.
4. Tang, H., Tian, Y., Wu, Z.S., Zeng, Y.J., Wang, Y., Hou, Y., Ye, Z., and Lu, J. (2022). AC Line Filter Electrochemical Capacitors: Materials, Morphology and Configuration. Energy & Environ. Materials *5*, 1060–1083.
5. Zhao, D., Jiang, K., Li, J., Zhu, X., Ke, C., Han, S., Kymakis, E., and Zhuang, X. (2020). Supercapacitors with alternating current line-filtering performance. BMC Mater. *2*, 3–23.
6. Li, Z., Wang, X., Zhao, L., Chi, F., Gao, C., Wang, Y., Yan, M., Zhou, Q., Zhao, M., Wang, X., et al. (2022). Aqueous hybrid electrochemical capacitors with ultra-high energy density approaching for thousand-volts alternating current line filtering. Nat. Commun. *13*, 6359.
7. Hu, Y., Wu, M., Chi, F., Lai, G., Li, P., He, W., Lu, B., Weng, C., Lin, J., Chen, F., et al. (2023). Ultralow-resistance electrochemical capacitor for integrable line filtering. Nature *624*, 74–79.
8. Huang, L., and Dai, L. (2017). On-Chip Microsupercapacitors Based on Coordination Polymer Frameworks for Alternating Current Line-Filtering. Angew. Chem. Int. Ed. Engl. *56*, 6381–6383.
9. Feng, X., Shi, X., Ning, J., Wang, D., Zhang, J., Hao, Y., and Wu, Z. (2021). Recent advances in micro-supercapacitors for AC line-filtering performance: From fundamental models to emerging applications. eScience *1*, 124–140.
10. Wang, F., Guo, Z., Wang, Z., Zhu, H., Zhao, G., Chen, C., Liu, M., Sun, R., Kang, F., Wong, C.P., et al. (2023). Laser-Induced Transient Self-Organization of TiN(x) Nano-Filament Percolated Networks for High Performance Surface-Mountable Filter Capacitors. Adv. Mater. *35*, 2210038.
11. Simon, P., and Gogotsi, Y. (2020). Perspectives for electrochemical capacitors and related devices. Nat. Mater. *19*, 1151–1163.
12. Simon, P., and Gogotsi, Y. (2008). Materials for electrochemical capacitors. Nat. Mater. *7*, 845–854.
13. Raccichini, R., Varzi, A., Passerini, S., and Scrosati, B. (2015). The role of graphene for electrochemical energy storage. Nat. Mater. *14*, 271–279.
14. Zhang, M., Dong, K., Saeedi Garakani, S., Khorsand Kheirabad, A., Manke, I., Wu, M., Wang, H., Qu, L., and Yuan, J. (2022). Bridged Carbon Fabric Membrane with Boosted Performance in AC Line-Filtering Capacitors. Adv. Sci. (Weinh) *9*, e2105072.
15. Zhao, M., Qin, Y., Wang, X., Wang, L., Jin, Q., Song, M., Wang, X., and Qu, L. (2023). PEDOT:PSS/Ketjenblack Holey Nanosheets with Ultrahigh Areal Capacitance for kHz AC Line-Filtering Micro-Supercapacitors. Adv. Funct. Mater. 2313495.
16. Xu, S., Wu, M., and Zhang, J. (2022). Ultrafast Electrochemical Capacitors with Carbon Related Materials as Electrodes for AC Line Filtering. Chemistry *28*, e202200237.
17. Rangom, Y., Tang, X.S., and Nazar, L.F. (2015). Carbon Nanotube-Based Supercapacitors with Excellent ac Line Filtering and Rate Capability via Improved Interfacial Impendance. ACS Nano *9*, 7248–7255.
18. Huang, P., Lethien, C., Pinaud, S., Brousse, K., Laloo, R., Turq, V., Respaud, M., Demortière, A., Daffos, B., Taberna, P.L., et al. (2016). On-chip and freestanding elastic carbon films for micro-supercapacitors. Science *351*, 691–695.
19. El-Kady, M.F., and Kaner, R.B. (2013). Scalable fabrication of high-power graphene micro-supercapacitors for flexible and on-chip energy storage. Nat. Commun. *4*, 1475.
20. Ellis, B.L., Knauth, P., and Djenizian, T. (2014). Three-dimensional self-supported metal oxides for advanced energy storage. Adv. Mater. *26*, 3368–3397.
21. Létiche, M., Eustache, E., Freixas, J., Demortière, A., De Andrade, V., Morgenroth, L., Tilmant, P., Vaurette, F., Troadec, D., Roussel, P., et al. (2017). Atomic Layer Deposition of Functional Layers for on Chip 3D Li-Ion All Solid State Microbattery. Adv. Energy Mater. *7*, 1601402.
22. Lethien, C., Le Bideau, J., and Brousse, T. (2019). Challenges and prospects of 3D micro-supercapacitors for powering the internet of things. Energy Environ. Sci. *12*, 96–115.
23. Brachet, M., Gaboriau, D., Gentile, P., Fantini, S., Bidan, G., Sadki, S., Brousse, T., and Le Bideau, J. (2016). Solder-reflow resistant solid-state micro-supercapacitors based on ionogels. J. Mater. Chem. A *4*, 11835–11843.
24. Fan, Z., Islam, N., and Bayne, S.B. (2017). Towards kilohertz electrochemical capacitors for filtering and pulse energy harvesting. Nano Energy *39*, 306–320.
25. Chi, F., Li, C., Zhou, Q., Zhang, M., Chen, J., Yu, X., and Shi, G. (2017). Graphene-Based Organic Electrochemical Capacitors for AC Line Filtering. Adv. Energy Mater. *7*, 1700591.
26. Korenblit, Y., Rose, M., Kockrick, E., Borchardt, L., Kvit, A., Kaskel, S., and Yushin, G. (2010). High-Rate Electrochemical Capacitors Based on Ordered Mesoporous Silicon Carbide-Derived Carbon. ACS Nano *4*, 1337–1344.
27. Zhang, M., Yu, X., Ma, H., Du, W., Qu, L., Li, C., and Shi, G. (2018). Robust graphene composite films for multifunctional electrochemical capacitors with an ultrawide range of areal mass loading toward high-rate frequency response and ultrahigh specific capacitance. Energy Environ. Sci. *11*, 559–565.
28. Yoo, Y., Kim, S., Kim, B., and Kim, W. (2015). 2.5 V compact supercapacitors based on ultrathin carbon nanotube films for AC line filtering. J. Mater. Chem. A *3*, 11801–11806.
29. Sheng, K., Sun, Y., Li, C., Yuan, W., and Shi, G. (2012). Ultrahigh-rate supercapacitors based on eletrochemically reduced graphene oxide for ac line-filtering. Sci. Rep. *2*, 247.
30. Xu, S., Wen, Y., Chen, Z., Ji, N., Zou, Z., Wu, M., Qu, L., and Zhang, J. (2021). Vertical Graphene Arrays as Electrodes for Ultra-High Energy Density AC Line-Filtering Capacitors. Angew. Chem. Int. Ed. Engl. *60*, 24505–24509.
31. Premathilake, D., Outlaw, R.A., Quinlan, R.A., Parler, S.G., Butler, S.M., and Miller, J.R. (2018). Fast Response, Carbon-Black-Coated, Vertically-Oriented Graphene Electric Double Layer Capacitors. J. Electrochem. Soc. *165*, A924–A931. Black.
32. Ren, G., Pan, X., Bayne, S., and Fan, Z. (2014). Kilohertz ultrafast electrochemical supercapacitors based on perpendicularly-oriented graphene grown inside of nickel foam. Carbon *71*, 94–101.
33. Lin, J., Zhang, C., Yan, Z., Zhu, Y., Peng, Z., Hauge, R.H., Natelson, D., and Tour, J.M. (2013). 3-Dimensional graphene carbon nanotube carpet-based microsupercapacitors with high electrochemical performance. Nano Lett. *13*, 72–78.
34. Gund, G.S., Park, J.H., Harpalsinh, R., Kota, M., Shin, J.H., Kim, T., Gogotsi, Y., and Park, H.S. (2019). MXene/Polymer Hybrid Materials for Flexible AC-Filtering Electrochemical Capacitors. Joule *3*, 164–176.
35. Sun, H., Mei, L., Liang, J., Zhao, Z., Lee, C., Fei, H., Ding, M., Lau, J., Li, M., Wang, C., et al. (2017). Three-dimensional holey-graphene/niobia composite architectures for ultrahigh-rate energy storage. Science *356*, 599–604.
36. Cai, M., Outlaw, R.A., Butler, S.M., and Miller, J.R. (2012). A high density of vertically-oriented graphenes for use in electric double layer capacitors. Carbon *50*, 5481–5488.
37. Li, Q., Sun, S., Smith, A.D., Lundgren, P., Fu, Y., Su, P., Xu, T., Ye, L., Sun, L., Liu, J., et al. (2019). Compact and low loss electrochemical capacitors using a graphite / carbon nanotube hybrid material for miniaturized systems. J. Power Sources *412*, 374–383.
38. Li, W., Azam, S., Dai, G., and Fan, Z. (2020). Prussian blue based vertical graphene 3D structures for high frequency electrochemical capacitors. Energy Stor. Mater. *32*, 30–36.
39. Liu, W., Feng, Y., Yan, X., Chen, J., and Xue, Q. (2013). Superior Micro-Supercapacitors Based on Graphene Quantum Dots. Adv. Funct. Mater. *23*, 4111–4122.
40. Wang, W., Tian, M., Abdulagatov, A., George, S.M., Lee, Y.C., and Yang, R. (2012). Three-dimensional Ni/TiO_2 nanowire network for high areal capacity lithium ion microbattery applications. Nano Lett. *12*, 655–660.
41. Tian, M., Wang, W., Liu, Y., Jungjohann, K.L., Thomas Harris, C., Lee, Y., and Yang, R. (2015). A three-dimensional carbon nano-network for high performance lithium ion batteries. Nano Energy *11*, 500–509.

42. Chang, W., Hsueh, Y.C., Huang, S.H., Liu, K.I., Kei, C.C., and Perng, T.P. (2013). Fabrication of Ag-loaded multi-walled TiO_2 nanotube arrays and their photocatalytic activity. J. Mater. Chem. A *1*, 1987–1991.

43. Nie, R., Miao, M., Du, W., Shi, J., Liu, Y., and Hou, Z. (2016). Selective hydrogenation of C C bond over N-doped reduced graphene oxides supported Pd catalyst. Appl. Catal. B *180*, 607–613.

44. Tamor, M.A., and Vassell, W.C. (1994). Raman "fingerprinting" of amorphous carbon films. J. Appl. Phys. *76*, 3823–3830.

45. Khakpour, I., Baboukani, A.R., Forouzanfar, S., Allagui, A., and Wang, C. (2021). In-situ exfoliation and integration of vertically aligned graphene for high-frequency response on-chip microsupercapacitors. J. Power Sources *516*, 230701.

46. Zhang, Z., Liu, M., Tian, X., Xu, P., Fu, C., Wang, S., and Liu, Y. (2018). Scalable fabrication of ultrathin free-standing graphene nanomesh films for flexible ultrafast electrochemical capacitors with AC line-filtering performance. Nano Energy *50*, 182–191.

47. Pech, D., Brunet, M., Durou, H., Huang, P., Mochalin, V., Gogotsi, Y., Taberna, P.L., and Simon, P. (2010). Ultrahigh-power micrometre-sized supercapacitors based on onion-like carbon. Nat. Nanotechnol. *5*, 651–654.

48. Mariappan, V.K., Krishnamoorthy, K., Manoharan, S., Pazhamalai, P., and Kim, S.J. (2021). Electrospun Polymer-Derived Carbyne Supercapacitor for Alternating Current Line Filtering. Small *17*, e2102971.

49. Ren, G., Li, S., Fan, Z.X., Hoque, M.N.F., and Fan, Z. (2016). Ultrahigh-rate supercapacitors with large capacitance based on edge oriented graphene coated carbonized cellulous paper as flexible freestanding electrodes. J. Power Sources *325*, 152–160.

50. Tang, H., Xia, K., Lu, J., Fu, J., Zhu, Z., Tian, Y., Wang, Y., Liu, M., Chen, J., Xu, Z., et al. (2021). $NiTe_2$-based electrochemical capacitors with high-capacitance AC line filtering for regulating TENGs to steadily drive LEDs. Nano Energy *84*, 105931.

51. Taberna, P.L., Simon, P., and Fauvarque, J.F. (2003). Electrochemical Characteristics and Impedance Spectroscopy Studies of Carbon-Carbon Supercapacitors. J. Electrochem. Soc. *150*, A292.

52. Fan, Y., Yi, Z., Song, G., Wang, Z., Chen, C., Xie, L., Sun, G., Su, F., and Chen, C. (2021). Self-standing graphitized hybrid Nanocarbon electrodes towards high-frequency supercapacitors. Carbon *185*, 630–640.

53. Wang, J., Wan, J., and Wang, D. (2019). Hollow Multishelled Structures for Promising Applications: Understanding the Structure-Performance Correlation. Acc. Chem. Res. *52*, 2169–2178.

54. Ye, J., Liu, L., Oakdale, J., Lefebvre, J., Bhowmick, S., Voisin, T., Roehling, J.D., Smith, W.L., Cerón, M.R., van Ham, J., et al. (2021). Ultra-low-density digitally architected carbon with a strutted tube-in-tube structure. Nat. Mater. *20*, 1498–1505.

55. Chen, C., Cao, J., Wang, X., Lu, Q., Han, M., Wang, Q., Dai, H., Niu, Z., Chen, J., and Xie, S. (2017). Highly stretchable integrated system for micro-supercapacitor with AC line filtering and UV detector. Nano Energy *42*, 187–194.

56. Strauss, V., Anderson, M., Turner, C.L., and Kaner, R.B. (2019). Fast response electrochemical capacitor electrodes created by laser-reduction of carbon nanodots. Mater. Today Energy *11*, 114–119.

57. Islam, N., Hoque, M.N.F., Li, W., Wang, S., Warzywoda, J., and Fan, Z. (2019). Vertically edge-oriented graphene on plasma pyrolyzed cellulose fibers and demonstration of kilohertz high-frequency filtering electrical double layer capacitors. Carbon *141*, 523–530.

58. Zhang, C., Du, H., Ma, K., and Yuan, Z. (2020). Ultrahigh-Rate Supercapacitor Based on Carbon Nano-Onion/Graphene Hybrid Structure toward Compact Alternating Current Filter. Adv. Energy Mater. *10*, 2002132.

59. Miller, J.R., and Outlaw, R.A. (2015). Vertically-Oriented Graphene Electric Double Layer Capacitor Designs. J. Electrochem. Soc. *162*, A5077–A5082.

60. Bo, Z., Xu, C., Yang, H., Shi, H., Yan, J., Cen, K., and Ostrikov, K. (2019). Hierarchical, Vertically-Oriented Carbon Nanowall Foam Supercapacitor using Room Temperature Ionic Liquid Mixture for AC Line Filtering with Ultrahigh Energy Density. ChemElectroChem *6*, 2167–2173.

61. Wang, S., Lin, L., Xie, Y., Jing, Q., Niu, S., and Wang, Z.L. (2013). Sliding-triboelectric nanogenerators based on in-plane charge-separation mechanism. Nano Lett. *13*, 2226–2233.

62. Islam, N., Li, S., Ren, G., Zu, Y., Warzywoda, J., Wang, S., and Fan, Z. (2017). High-frequency electrochemical capacitors based on plasma pyrolyzed bacterial cellulose aerogel for current ripple filtering and pulse energy storage. Nano Energy *40*, 107–114.